Alexandria Engineering Journal (2019) 58, 519–529

HOSTED BY

Alexandria University

Alexandria Engineering Journal

www.elsevier.com/locate/aej
www.sciencedirect.com

ORIGINAL ARTICLE

Thermal stability and entropy generation of unsteady reactive hydromagnetic Powell-Eyring fluid with variable electrical and thermal conductivities

S.O. Salawu [a,*], A.R. Hassan [b], A. Abolarinwa [a], N.K. Oladejo [a]

[a] Department of Mathematics, Landmark University, Omu-aran, Nigeria
[b] Department of Mathematics, Tai Solarin University of Education, Ijagun, Nigeria

Received 8 January 2019; revised 29 January 2019; accepted 12 May 2019
Available online 10 June 2019

KEYWORDS

Thermal runaway;
Reactive fluid;
Chemical kinetic;
Variable conductivity;
Non-Newtonian

Abstract Theoretical analysis of thermal stability and inherent irreversibility of reactive hydromagnetic Powell-Eyring fluid flow in a fixed vertical channel with variable electrical and thermal conductivities is examined. The conducting reactive fluid is influenced by gravity and axial pressure gradient under bimolecular kinetic rate law. Ignoring the material assumptions, the governing dimensionless equations are solved by finite semi-discretization difference scheme along with integration Fehlberg Runge-Kutta method. The results for the momentum and heat equations, Bejan number, thermal runaway, entropy generation and current density are graphically presented under different thermophysical parameters. The computational results for the shear stress and heat transfer at the wall is also presented and discussed quantitatively. It was observed that the parameter which enhance the rate of entropy generation also augment Bejan number with large pitch ratio. Hence, entropy generation can be minimized at low dissipation and material variables.

1. Introduction

A convective laminar flow is a fluid flow motion originated solely owing to differences in density during heating or cooling of fluids. It can also arise due to differences in both temperature gradient and species concentration. The study of reactive combustion flow is significant in environmental and industrial applications such as atmospheric flows, thermal regulation, cooling of electronic devices, nuclear reactor, thermal hydraulics and frost formation, Rana et al. [20]. The importance of chemical reactive fluid flow in the production of polymer extrusion, fiber and many more cannot be over emphases as it depends on the rate of heat transfer. Reactive hydromagnetic non-Newtonian flow fluid is very important in several processes such as slurries, paper pulp, paints, suspension granular, shampoos solutions and some oils are of non-Newtonian fluid, Salawu [35].

Several researchers under diverse physical conditions have developed an interest in the study of different models of

* Corresponding author.
E-mail address: salawu.sulyman@lmu.edu.ng (S.O. Salawu).
Peer review under responsibility of Faculty of Engineering, Alexandria University.

https://doi.org/10.1016/j.aej.2019.05.004

Nomenclature

$\bar{u}, w$	dimensional and dimensionless fluid velocity, ms^{-1}
$\bar{y}, y$	dimensional and dimensionless perpendicular flow direction, m
A	constant reaction rate
h	channel of width, m
B_0	magnetic field strength, Wbm^{-2}
Br	Brinkman number
C	reactant species
C_p	specific heat at constant pressure, $Jkg^{-1}\ K^{-1}$
g	acceleration due to gravity, ms^{-2}
Gr	thermal Grashof number
G	pressure gradient
$\overline{P}$	dimensional fluid pressure, Pa
$\bar{x}$	dimensional flow direction, m
T	dimensional fluid temperature, K
Q	heat reaction, W
n	chemical kinetics
Pr	Prandtl number
l	Planck's number
k	thermal conductivity, $Wm^{-1}\ K^{-1}$
Q	heat of reaction term
R	universal gas constant
T_a	wall temperature, K
v	vibration frequency
Ha	Hartmann number
c	variable thermal conductivity

Greek symbol

ϵ	activation energy
β	thermal expansion coefficient, $K^{?1}$
α, δ	Powell-Eyring fluid material
θ	dimensionless fluid temperature, K
μ	fluid viscosity, $kgm^{-1}\ s^{-1}$
ϕ	electric field loading
σ	electrical conductivity
ρ	fluid density, kgm^{-3}
λ	Frank-Kamenetskii term

non-Newtonian fluids due to it fabulous applications in numerous manufacturing and industrial processes. Thus, Mustafa [33] carried out analytical analysis of Buongiorno model in a nanofluid with zero net particle flux. Hayat et al. [16] studied the boundary layer nanofluid flow of second grade with heat sink and radiation. They used similarity techniques to solve the three dimensional flow through an elongating surface and obtained the analytical solutions by employing Homotopy method. Ghadikolaei et al. [8], Rashidi et al. [34], Kareem et al. [21] presented the approximated analytic and computational results for the flow of micropolar fluid and energy transfer past permeable media. Analysis of viscoelastic flow and heat transport past an expanding sheet was examined by Cortell [6]. A multi-dimensional and time dependent Maxwell flow liquid through a broadening plate was reported by Awais et al. [2]. In their study, the analytical solutions of the unsteady modeled multi-dimensional velocity equation of Maxwell fluid was obtained. Gireesha and Mahanthesh [11] investigated the convective flow of unsteady heat transfer of Walters-B fluid and hall effect in a permeable medium. Ghadikolaei et al. [9], Makinde and Chinyoka [29] and Salawu et al. [36] analysed the flow of third-grade reactive hydromagnetic fluid with asymmetric cooling. It was reported from the study that the non-Newtonian parameter enhances the fluid viscosity which in turn decreases the flow rate. Mahmood et al. [26] studied optimal solution of Jeffery oblique stagnation fluid flow over a stretching sheet while Mustafa [32] reported on anomalous nanofluid flow in a circlular pipe with heat transfer enhancement.

Of the models of non-Newtonian liquids, the fluid model for the Powell-Eyring has a better improvement over other non-Newtonian fluids. Apart from the fact that it was obtained from the kinetic liquid theory, unlike Power-law liquid model that was deduced from empirical relation, Powell-Eyring fluid can behave like a Newtonian fluid at high and low shear rate. In view of these, Gholinia et al. [10] investigated the impact of heterogeneous-homogeneous reactions on Powell-Eyring MHD past a rotating disk. Jalil et al. [19] considered the flow of Powell-Eyring heat transfer fluid over an unceasingly moving porous plate with free rivulet. In the study, the core model was transformed to an ordinary differential equation by employing a Lie group and then solved computationally by applying the Keller-box technique. Powell-Eyring boundary layer flow with variable viscosity in an elongating cylinder was examined by Malik et al. [31]. Akbar et al. [1] studied the computational solution of hydromagnetic Eyring-Powell flow in a boundary layer past an extending sheet. Mahanthesh et al. [25] considered transient Joule heating fluid of nano Powell-Eyring heat transfer in a magnetohydromagnetic flow with thermal dissipation and radiation. The authors used similarity quantities to transform the main equation and then utilized shooting method coupled with Fehlberg Runge-Kutta techniques to obtain the numerical results. From the results, it was reported that the Powell-Eyring term stimulated the flow as it discourages the fluid opposing forces. All the above studies was done without considering the rate of entropy generation in the system.

Global degradation in the energy resource has pushed nations and researchers into the quest for the preservation of energy and boosting of the existing energy system. The scientists developed new plans with the goal of mitigating or eliminating available work destruction. The new approach gave birth to thermodynamics second law which measure the system thermal irreversibility process in terms entropy generation rate; Salawu and Okedoye [37]. Entropy generation is caused by irreversibility process in many thermal engineering systems such as optical switches, heat exchangers, turbo machinery, peristaltic MHD compressor and so on. This irreversibility process reduces the efficiency of the machine; Hassan and Gbadeyan [14] and Khan et al. [23]. Several research has been done on how to minimize the effect of entropy generation. Khan et al. [23] reported on minimization of entropy genera-

tion with thermal radiation and moving thin needle on nanofluid flow using Shooting method. It was noticed from their study that drags force encourages copper nanoparticle but leads to aluminum oxide nanoparticle decay. Minimization of entropy production of a viscoelastic magnetohydrodynamic fluid flow in porous media was examined by Baag et al. [3]. It was observed from their results that increasing viscoelastic and magnetic variables diminish the velocity field. Among many other scholars that have contributed to the study of the effect of entropy generation are [2,17,38]. With numerous works done on entropy generation, to our best of knowledge, no researcher has considered entropy generation and thermal criticality of a reactive Powell-Eyring fluid with variable properties.

The purpose of this study is to investigate the thermal runaway and inherent irreversibility of a reactive powell-Eyring fluid with variable electrical and thermal conductivities via thermodynamic second law. The liquid flows in a fixed vertical wall in the presence of a magnetic field. The equations satisfying the temperature, current density, velocity, Bejan number, entropy generation, shear stress and heat gradient are expressed and solved. Flow mathematical model is reported in Section two while Section 3 discussed the entropy generation analysis. In Section 4, the finite difference of semi-implicit numerical scheme is implemented in the solution process. Graphical results are presented and discussed qualitatively with respect to various parameters embedded in the system in Section 5.

2. Mathematical formulation

Consider a transient incompressible Poiseuille flow of conducting reactive Powell-Eyring fluid with exponential variable thermal conductivity and temperature dependent variable electrical conductivity. The induced magnetic field strength B_0 is influenced by electric field E_f. The reactive non-Newtonian fluid flows through fixed vertical walls of width h is stimulated by gravity. The temperature of the fixed walls is non-uniform as presented in Fig. 1. The model is by the Bimolecular kinetic law with $n = 0.5$ and at $\bar{t} \leqslant 0$, the fluid is assumed static with the exothermic heat, but the chemical reactive fluid is encouraged by the fully developed axial uniform pressure gradient at $\bar{t} > 0$. The viscoelastic effect is stimulated by the employment of non-Newtonian Powell-Eyring Cauchy model. The induced magnetic field is ignored due to negligible of the Reynolds number.

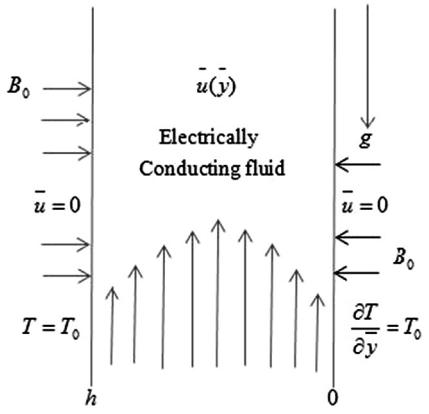

Fig. 1 The model geomentry.

The heat dependent variable electrical conductivity $\sigma(T)$ for the reactive fluid is defined as

$$\sigma(T) = \sigma_0 \left(\frac{E(T - T_0)}{RT_0^2} \right)^r. \tag{1}$$

The term r is the electrical conductivity exponent and σ_0 is the electrical conductivity of the plate. The fluid model for Cauchy Eyring-Powell stress tensor according to Hayat et al. [15] is defined as

$$S_{ij} = \frac{1}{\Lambda} sinh^{-1}\left(\frac{1}{\tau} \frac{\partial \bar{u}_i}{\partial \bar{x}_j} \right) + \mu \frac{\partial \bar{u}_i}{\partial \bar{x}_j}. \tag{2}$$

The parameter τ and Λ are the fluid material constant while μ is the coefficient of fluid viscosity. That is,

$$sinh^{-1}\left(\frac{1}{\tau} \frac{\partial \bar{u}_i}{\partial \bar{x}_j} \right) \cong \frac{1}{\tau} \frac{\partial \bar{u}_i}{\partial \bar{x}_j} - \frac{1}{6} \left(\frac{1}{\tau} \frac{\partial \bar{u}_i}{\partial \bar{x}_j} \right)^3. \tag{3}$$

Follow the assumptions above, the dimensional boundary layer approximations for the velocity and heat balance governing equations of the reactive Powell-Eyring fluid with variable properties [4,24] are as follows:

$$\rho \frac{\partial \bar{u}}{\partial \bar{t}} = -\frac{\partial \overline{P}}{\partial \bar{x}} + \left(\mu + \frac{1}{\Lambda\tau} \right) \frac{\partial^2 \bar{u}}{\partial \bar{y}^2} - \frac{1}{2\Lambda\tau^3} \left(\frac{\partial \bar{u}}{\partial \bar{y}} \right)^2 \frac{\partial^2 \bar{u}}{\partial \bar{y}^2} - \sigma(T) B_0 \left(B_0 \bar{u} + E_f \right) + g\beta(T - T_0). \tag{4}$$

$$\rho C_p \frac{\partial T}{\partial \bar{t}} = k(T) \frac{\partial^2 T}{\partial \bar{y}^2} + \frac{\partial T}{\partial \bar{y}} \frac{\partial k(T)}{\partial \bar{y}} + QCA \left(\frac{KT}{vl} \right)^n e^{\frac{E}{RT}} + \left(\frac{\partial \bar{u}}{\partial \bar{y}} \right)^2 \left[\left(\mu + \frac{1}{\Lambda\tau} \right) - \frac{1}{6\Lambda\tau^3} \left(\frac{\partial \bar{u}}{\partial \bar{y}} \right)^2 \right] + \sigma(T) \left(B_0 \bar{u} + E_f \right)^2 \tag{5}$$

The governing equations are subjected to the boundary conditions

$$\begin{aligned} &\bar{u}(\bar{y}, 0) = 0, \quad T(\bar{y}, 0) = T_a, \\ &\bar{u}(h, \bar{t}) = 0, \quad T(h, \bar{t}) = T_0 \quad \text{for } \bar{t} > 0, \\ &\bar{u}(0, \bar{t}) = 0, \quad \frac{\partial T}{\partial \bar{y}}(0, \bar{t}) = T_0 \quad \text{for } \bar{t} > 0. \end{aligned} \tag{6}$$

Follow Makinde and Franks [29], the exponentially varied thermal conductivity $k(T)$ is taken as

$$k(T) = k_0 e^{a(T - T_0)}. \tag{7}$$

The term a can be positive for some liquids like water vapour or air or negative for benzene and others. The following quantities in Eq. (8) are introduced into the equations above.

$$\begin{aligned} &x = \frac{\bar{x}}{h}, t = \frac{\mu \bar{t}}{h^2 \rho}, y = \frac{\bar{y}}{h}, G = -\frac{\partial P}{\partial x}, \theta = \frac{E(T - T_0)}{RT_0^2}, \\ &Ha = \frac{h^2 \sigma_0 B_0^2}{\mu}, w = \frac{\bar{u}}{U}, P = \frac{\overline{P}h}{U\mu}. \end{aligned} \tag{8}$$

The main equations and the boundary conditions in dimensionless form become

$$\frac{\partial w}{\partial t} = \frac{\partial^2 w}{\partial y^2} + \alpha \frac{\partial^2 w}{\partial y^2} - \delta\alpha \left(\frac{\partial w}{\partial y} \right)^2 \frac{\partial^2 w}{\partial y^2} - Ha(\phi + w)\theta^r + G + Gr\theta, \tag{9}$$

$$Pr\frac{\partial\theta}{\partial t} = e^{c\theta}\frac{\partial^2\theta}{\partial y^2} + ce^{c\theta}\left(\frac{\partial\theta}{\partial y}\right)^2 + Br\left[\left(\frac{\partial w}{\partial y}\right)^2\left((1+\alpha)+\frac{\alpha\delta}{3}\left(\frac{\partial w}{\partial y}\right)^2\right) + Ha(w+\phi)^2\theta^r\right] + \lambda(1+\epsilon\theta)^n e^{\frac{\theta}{1+\epsilon\theta}}, \tag{10}$$

The dimensionless boundary conditions

$$w(y,0)=0,\quad \theta(y,0)=\theta_a, w(0,t)=0,\quad \frac{\partial\theta}{\partial y}(0,t)=0,\quad \text{for} t>0, w(1,t)=0,\quad \theta(1,t)=0,\quad \text{for } t>0. \tag{11}$$

where $\alpha=\frac{1}{\mu\Lambda\tau}, \delta=\frac{U^2}{2\tau^2h^2}, \lambda=\frac{AQCh^2E}{Rk_0T_0^2}\left(\frac{KT_0}{vl}\right)^n e^{-\frac{1}{\epsilon}}, Br=\frac{\mu EU^2}{Rk_0T_0^2}, Pr=\frac{\mu c_p}{k_0}, \epsilon=\frac{RT_0}{E}, c=\frac{aRT_0^2}{E}, Gr=\frac{g\beta h^2RT_0}{\mu U}, \theta_a=\frac{E(T_a-T_0)}{RT_0^2}, \phi=\frac{E_f}{UB_0}, Ha=\frac{h^2\sigma_0B_0^2}{\mu}$ as defined in the nomenclature.

The quantities of engineering interest are the coefficient of skin friction and Nusselt number defined as;

$$C_f=\left.\frac{\partial w}{\partial y}\right|_{y=0,1},\quad Nu=-\left.\frac{\partial\theta}{\partial y}\right|_{y=0,1}. \tag{12}$$

The total generated current and the current density within the flow system for the reactive hydromagnetic fluid are as follows;

$$I_T=\int_0^1(\phi+w)\theta^r dy\quad (\text{Totalgeneratedcurrent})I_d = (\phi+w)\theta^r\quad (\text{Currentdensity}) \tag{13}$$

It is essential to consider that, for configuration of a short circuit where loading electric field is absent, $\phi=0$.

3. Analysis of entropy generation

The inherently irreversible of convective hydromagnetic Poiseuille flow in a vertical channel creates continuous entropy generation. This can be as a result of energy exchange between the channel walls and conducting Powell-Eyring fluid. The local entropy generation volumetric rate for the viscous fluid for an induced electric and magnetic fields is obtained as [9,37];

$$I_G=\frac{k(T)}{T_0^2}\left(\frac{dT}{d\bar{y}}\right)^2+\frac{\mu}{T_0}\left[\left(1+\frac{1}{\rho\Lambda\tau}\right)\left(\frac{d\bar{u}}{d\bar{y}}\right)^2-\frac{1}{6\rho\Lambda\tau^3}\left(\frac{d\bar{u}}{d\bar{y}}\right)^4\right]+\frac{\sigma(T)\left(B_0\bar{u}+E_f\right)^2}{T_0}. \tag{14}$$

The irreversibility heat transfer is described in the first term of Eq. (14) while the irreversibility as a result of magnetic field and fluid friction is respectively presented in the second and third terms of the equation. Using Eq. (8), the non-dimensional rate of entropy generation in Eq. (14) becomes

$$N_s=\frac{E^2h^2I_G}{k_0R^2T_0^2}=e^{c\theta}\left(\frac{d\theta}{dy}\right)^2+\frac{Br}{\epsilon}\left[(1+\alpha)\left(\frac{dw}{dy}\right)^2-\frac{\alpha\delta}{3}\left(\frac{dw}{dy}\right)^4+Ha(\phi+w)^2\theta^n\right], \tag{15}$$

Let $N_1=e^{c\theta}\left(\frac{d\theta}{dy}\right)^2$ and $N_2=\frac{Br}{\epsilon}\left[(1+\alpha)\left(\frac{dw}{dy}\right)^2-\frac{\alpha\delta}{3}\left(\frac{dw}{dy}\right)^4+Ha(\phi+w)^2\theta^n\right]$,

The Bejan number (Be) is defined as

$$Be=\frac{N_1}{N_s}=\frac{1}{1+\psi}, \tag{16}$$

where $\psi=\frac{N_2}{N_1}, N_s=N_2+N_1$ and N_1 depicts the heat transfer irreversibility, N_2 denotes the magnetic field and fluid friction irreversibility and ψ represents the irreversibility ratio.

The Bejan number (Be) ranges from $0\leqslant Be\leqslant 1$. Irreversibility due to magnetic field and fluid friction effects dominates the system when $Be=0$, but irreversibility as a result of heat transfer controlled the reactive flow system when $Be=1$ due to heat differences.

4. Numerical analysis

The computational scheme adopted is founded on finite difference of semi-implicit technique [3,18]. Implicit terms are intermediary considered at the level of time $(N+\zeta)$, for range $[0,1]$. Based on Cartesian linear uniform grid and mesh, the dimensionless equations are discretization on which finite differences are assumed. The central second order difference is used on the spatial derivatives for the first and second approximate. The boundary conditions are integrated by modifying the resultant last and first equations grid points. The momentum module for the semi-implicit system is expressed as:

$$\frac{w^{(N+1)}-w^{(N)}}{\Delta t}=(1+\alpha)\frac{\partial^2}{\partial y^2}w^{(N+\zeta)}+G+Gr(\theta)^{(N)}-\alpha\delta\left(\frac{\partial w}{\partial y}\right)^{2(N)}\frac{\partial^2}{\partial y^2}w^{(N+\zeta)}-Ha\left(\phi+w^{(N+\zeta)}\right)(\theta^r)^{(N)}. \tag{17}$$

The equation defining $w^{(N+1)}$ is written as:

$$-q_1w_{j-1}^{(N+1)}+\left(\Delta tHa(\theta^r)^{(N)}+2q_1\right)w_j^{(N+1)}-q_1w_{j+1}^{(N+1)} = \Delta t(1-\zeta)(1+\alpha)w_{yy}^{(N)}+w^{(N)}+\Delta tGr\theta^{(N)}+\Delta tG - \Delta t(1-\zeta)\alpha\delta\left(w_y\right)^{2(N)}w_{yy}^{(N)} - \Delta tHa(1-\zeta)\left(\phi+w^{(N)}\right)(\theta^r)^{(N)}. \tag{18}$$

where $q_1=\zeta\frac{\Delta t}{\Delta y^2}$ and its improve the consistence in time at $\zeta=\frac{1}{2}$ to second order. The solution scheme reduces to tri-diagonal inverse matrices. The integration scheme of semi-implicit for heat balance equation module resemble that of velocity module. The second unmixed derivatives for the energy reads:

$$Pr\frac{\theta^{(N+1)}-\theta^{(N)}}{\Delta t}=e^{c\theta^{(N)}}\frac{\partial^2}{\partial y^2}\theta^{(N+\zeta)}+c\left(e^{c\theta}\left(\frac{\partial\theta}{\partial y}\right)^2\right)^{(N)}+\lambda\left[(1+\epsilon\theta)^ne^{\frac{\theta}{1+\epsilon\theta}}\right]^{(N)}+Br\left[\left(\frac{\partial w}{\partial y}\right)^2\left((1+\alpha)+\frac{\alpha\delta}{3}\left(\frac{\partial w}{\partial y}\right)^2\right)+Ha(w+\phi)^2\theta^r\right]^{(N)}. \tag{19}$$

The equation defining $\theta^{(N+1)}$ becomes:

$$-q_1\theta_{j-1}^{(N+1)} + (Pr + 2q_1)\theta_j^{(N+1)} - q_1\theta_{j+1}^{(N+1)} = \lambda\left[(1+\epsilon\theta)^n e^{\frac{\theta}{1+c\theta}}\right]^{(N)} + \theta^{(N)} + \left(e^{c\theta}\theta_{yy}\right)^{(N)} + Br\left[(w_y)^2\left((1+\alpha) + \frac{\alpha\delta}{3}(w_y)^2\right) + Ha(\phi+w)^2\theta^r\right]^{(N)} + c\left(e^{c\theta}(\theta_y)^2\right)^{(N)}. \quad (20)$$

The solution scheme reduce to tri-diagonal inverse matrices. The procedures (18) and (20) are second order in space but consistence and accurate in first order at $\zeta = 1$. Here, $\zeta = 1$ is chosen for steady convergent solutions at high time steps.

5. Results and discussion

The impact of some arbitrarily chosen thermophysical parameter values of previous studies on the momentum, temperature, thermal criticality, energy, Bejan number, entropy generation, current density, skin friction and heat gradient is presented in Figs. 2, 3, 4,5, 6, 7, 8, 9, 10, 11, 12, 13, 14, 15, 16, 17, 8, 19 and 20 and Tables 1 and 2. The Prandtl computational number is assumed to range from [1,14] for fluids with exponential heat dependent thermal conductivity. Table 1 depicts the effects of rising in some parameter values on the flowing fluid and temperature at the channel wall. The parameters G, Gr, Br and λ respectively increase the shear stress and heat gradient at the wall due to enhancement in the momentum and temperature boundary layers that reduce the quantity of heat diffusion out of the system which in turn discourages fluid bonding forces. The parameters Ha and ϕ respectively decrease the skin friction and boosts the Nusselt number as portrayed in the table.

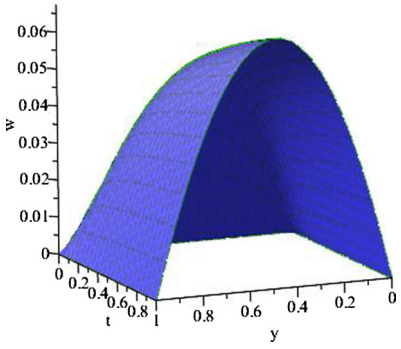

Fig. 2 3D Velocity profile with rising time.

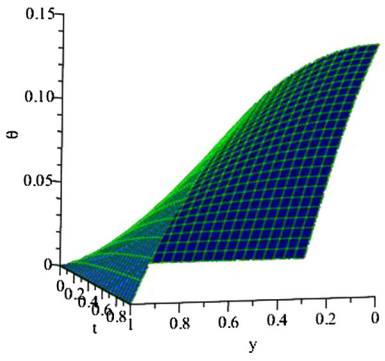

Fig. 3 3D Heat profile with rising time.

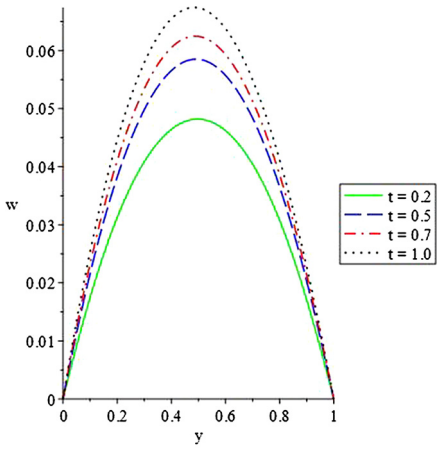

Fig. 4 Velocity profile with rising time.

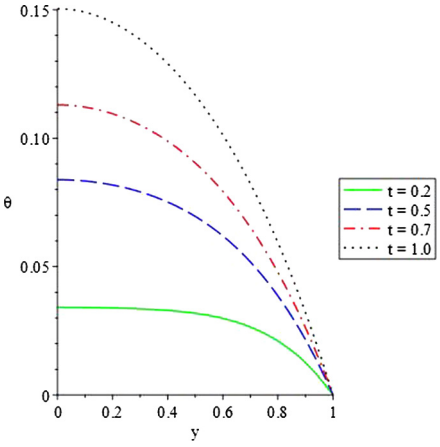

Fig. 5 Heat profile with rising time.

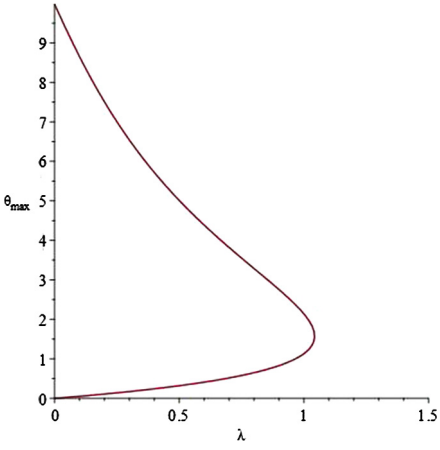

Fig. 6 Slice Approximate bifurcation.

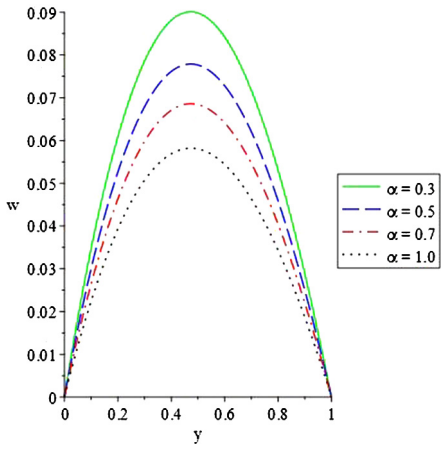

Fig. 7 Velocity profile with rising α.

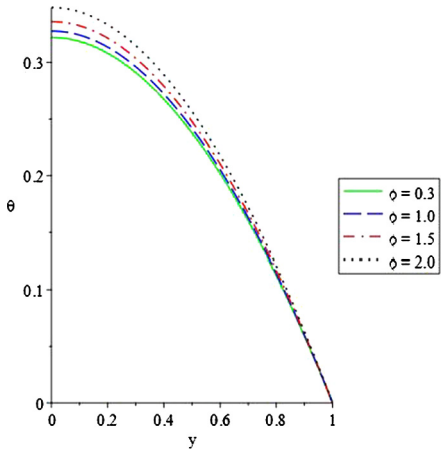

Fig. 10 Heat profile with rising ϕ.

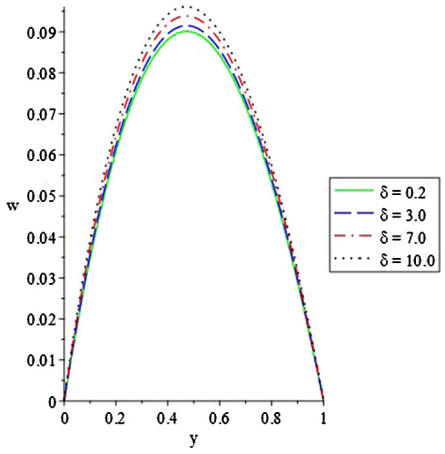

Fig. 8 Velocity profile with rising δ.

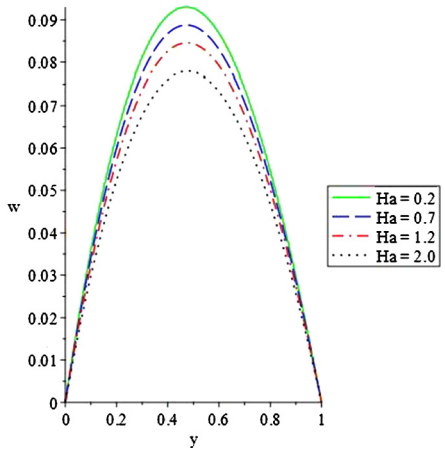

Fig. 11 Velocity profile with rising *Ha*.

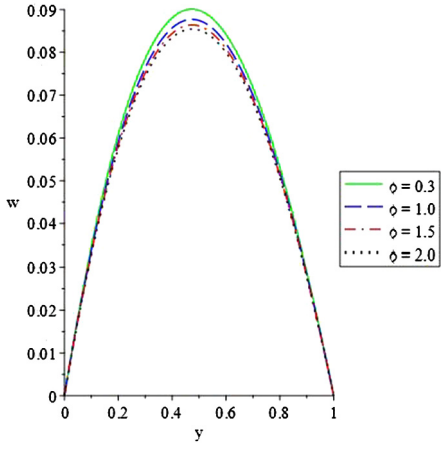

Fig. 9 Velocity profile with rising ϕ.

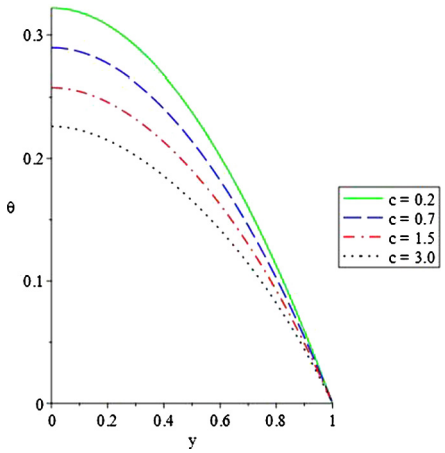

Fig. 12 Heat profile with rising *c*.

Table 2 represent the computational values for the thermal criticality results which describe and onset instability and thermal runaway in the reactive Powell-Eyring fluid under investigation. It gives estimate under different parameters and chemical kinetics of the critical regions called blowup. It is observed that the thermal criticality magnitude decreases that in turn encourages thermal stability with rises in the values of *Gr*, ϕ, *Br*, and *Ha*. But values of *c* and ϵ enhances the thermal

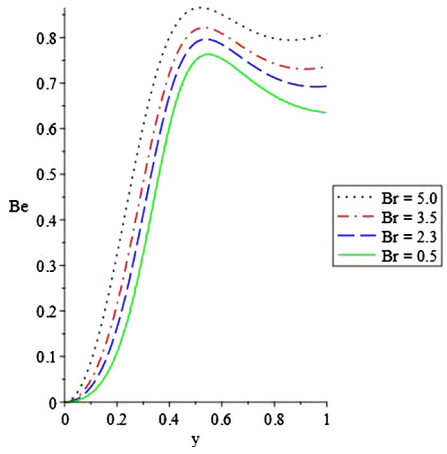

Fig. 13 Bejan number with rising *Br*.

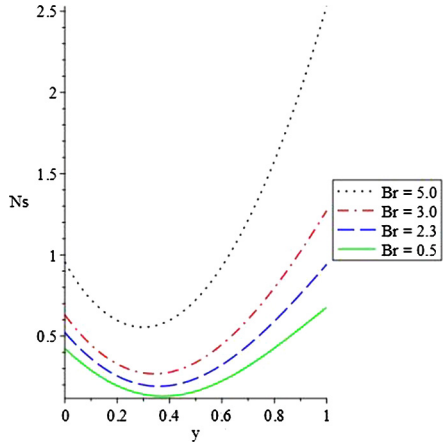

Fig. 14 Entropy generation with rising *Br*.

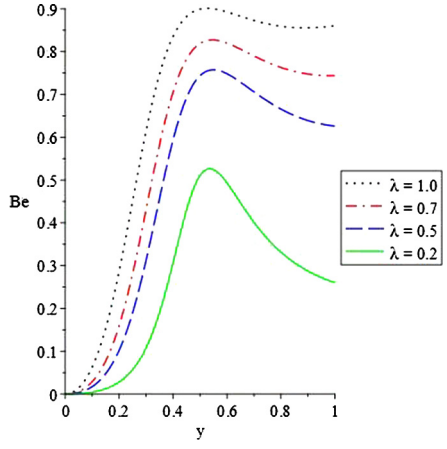

Fig. 15 Bejan number with rising λ.

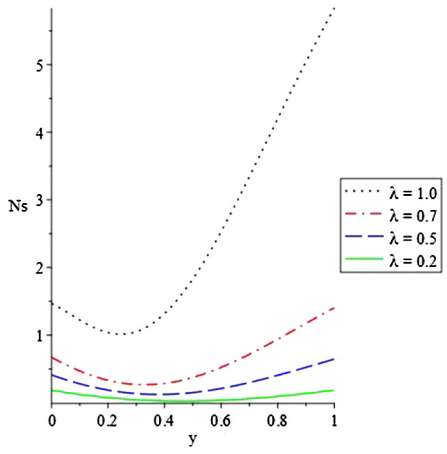

Fig. 16 Entropy generation with rising λ.

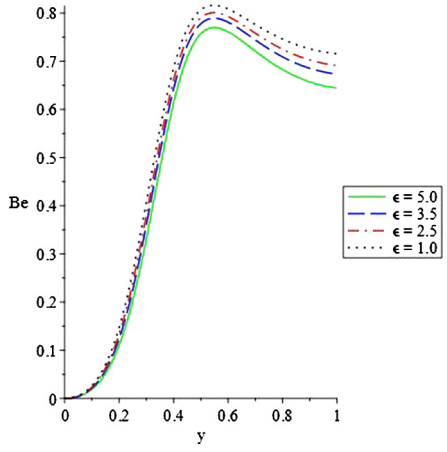

Fig. 17 Bejan number with rising ϵ.

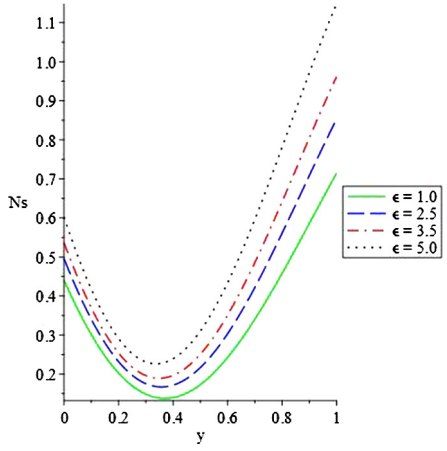

Fig. 18 Entropy generation with rising ϵ.

criticality magnitude that leads to thermal instability of the reactive Powell-Eyring fluid flow. Hence, the term λ needs to be consciously monitored to avoid blowup effect. Table 3 describes the comparison of the computational values for the heat distribution under different solution techniques, a special case of the present study. The results expressed the strength of the method used in the present study. Integration Fehlberg Runge-Kutta method is a numerical method of solution to dif-

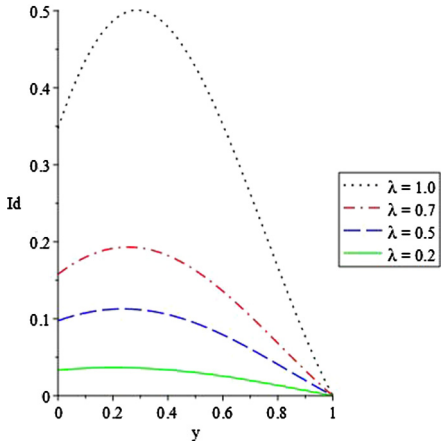

Fig. 19 Current density with rising λ.

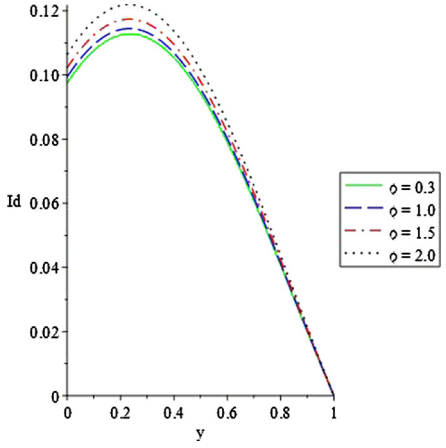

Fig. 20 Current density with rising ϕ.

ferential equations with average differences of order $10^{?3}$. From the results, a decrease in the numerical values is noticed along the flow direction from rest towards the to the other channel wall.

Figs. 2–5 illustrate the time variation on the rate of fluid flow and heat field across the vertical fixed channel. From its zero state, defined on even finer mesh, the velocity of the fluid rises steadily until it reaches the maximum state at the centre-line of the channel as seen in the Figs. 2 and 4. Similarly, the temperature of the fluid is enhanced as the time of evolution increases. The increment in the heat content as in the plots 3 and 4 is due the influence of the thermal boundary conditions and heat source terms. The time of obtaining the steady state for the velocity and temperature vary as it depends on the parameter values.

In Fig. 6, thermal criticality that is embodied by the Frank-Kamenenetskii term λ_c is demonstrated. For $\lambda > \lambda_c$, the steady solution varnish, but displayed a classical result denoting thermal runaway conditions at $\frac{d\lambda}{d\theta_{max}} = 0$. From the plot, it is seen that there exists a turning point that corresponds to the values of λ_c. Table 2 shows the computed values λ_c and θ_{max} for the various fluid parameters under different kinetics. Lower and upper branches of solutions are obtained as a result of the chemical kinetics in the energy equation.

The response of the fluid velocity to change in the material parameters α and δ is demonstrated in Figs. 7 and 8. From the plot 7, a noteworthy decrease in the fluid velocity is noticed as the material parameter α increases. This is because the term α stimulates the fluid viscosity which resists the free flow of reactive non-Newtonian fluid in the vertical channel. In the plot 8, a steady rise in the fluid flow rate towards the center of the channel is seen as the material parameter δ increases. The fluid particles can move faster and freely due to a reduction in the fluid bonding force that in turn boosted the flow rate.

The reaction of the fluid momentum and heat field to an increase in the fluid electric field loading ϕ is presented in Figs. 9 and 10. A decrease in both the fluid velocity and heat energy in the vertically fixed channel is observed. The behaviour is because the electric field loading induced a dragging force in an electrically conducting fluid that opposes the heat generating terms in the velocity and energy equations. As a result, the fluid viscosity is encouraged and thereby causes decrease in both the flow rate and temperature distributions. Fig. 11 depicts the impact of magnetic field *Ha* on the velocity distribution. The parameter *Ha* reduces the flow rate due to the Lorenz force influence that discourages the velocity equation source terms and thereby diminishes the overall flow rate. In Fig. 12, the temperature within the system decreases coupled with the reduction in the fluid viscosity as the thermal conductivity term rises. Consequently, the exothermic reaction

Table 1 Effects of some parameters (P) on $w_y(0)$ and $\theta_y(0)$ at the wall.

P	values	$w_y(0)$	$\theta_y(0)$	P	*values*	$w_y(0)$	$\theta_y(0)$
G	0.3	0.31468	0.32235	Br	0.5	0.39930	0.33522
	0.5	0.39309	0.32459		2.3	0.44715	0.41705
	0.7	0.47202	0.32735		3.5	0.49742	0.50277
	1.0	0.59152	0.33250		5.0	0.64160	0.74704
Ha	0.2	0.39309	0.32459	λ	0.2	0.26130	0.11127
	0.7	0.37548	0.32626		0.5	0.39309	0.32459
	1.2	0.35796	0.32791		0.7	0.51728	0.52592
	2.0	0.33009	0.33052		1.0	0.90974	1.15862
Gr	0.5	0.23687	0.32085	ϕ	0.3	0.39309	0.32459
	1.0	0.28844	0.32190		1.0	0.38225	0.33115
	1.5	0.34048	0.32314		1.5	0.37663	0.34050
	2.0	0.39309	0.32459		2.0	0.37274	0.35444

Table 2 Thermal criticality computational values for different chemical kinetics.

Gr	ϕ	Br	Ha	c	ϵ	n	λ_c	θ_{max}
0.2	0.3	0.2	0.2	0.2	0.1	−2.0	1.5790103149	2.5099983417
0.7	0.3	0.2	0.2	0.2	0.1	−2.0	1.5776290894	2.5197423588
0.5	1.0	0.2	0.2	0.2	0.1	−2.0	1.5561177062	2.5533557448
0.5	2.0	0.2	0.2	0.2	0.1	−2.0	1.4896695282	2.5890325540
0.5	0.3	2.3	0.2	0.2	0.1	0.0	1.1425503540	1.7830275310
0.5	0.3	3.5	0.2	0.2	0.1	0.0	1.1268271861	1.8323500658
0.5	0.3	0.2	0.7	0.2	0.1	0.0	1.1653733287	1.8173429278
0.5	0.3	0.2	2.0	0.2	0.1	0.0	1.1541533965	1.7584644632
0.5	0.3	0.2	0.2	0.3	0.1	0.5	1.0602648133	1.5425684654
0.5	0.3	0.2	0.2	0.5	0.1	0.5	1.0715338657	1.4373224463
0.5	0.3	0.2	0.2	0.2	0.2	0.5	1.0394568641	1.5483205265
0.5	0.3	0.2	0.2	0.2	0.5	0.5	1.0690486514	2.8317726315

Table 3 Comparison of the computational results for temperature profile. $\lambda = 0.5,\ Ha = 1,\ G = 1,\ \epsilon = 1,\ Br = 1,\ \alpha = \delta = \phi = Gr = Pr = r = c = 0$.

y	PM [27]	ADM [12]	Present study
0.00	0.3544502181	0.3581076494	0.358215990
0.25	0.3323243479	0.3358417798	0.335889705
0.50	0.2660663845	0.2691056991	0.269092738
0.75	0.1556934861	0.1577379743	0.157745281
1.00	0.0000000000	0.0002178316	0.000019253

decreases as the viscous heating strength diminishes, which then leads to overall drops in the temperature of the reactive Powell-Eyring fluid.

The Bejan number and entropy generation profile for rising in the Brinkman number term are reported in Figs. 13 and 14. Brinkman number conducts heat from the fixed walls to the viscous flowing fluid, it is the dissipative viscous heat generation and heat transfer through molecular conduction. Increasing Brinkamn number, reduces conducting heat due to viscous dissipation and leads to high Bejan number and heat irreversibility within the exothermic non-Newtonian fluid system. In Figs. 15 and 16, a significant rise in the Bejan number and heat irreversibility is noticed as the Frank-Kamenenetskii term λ is enhanced under the influence of gravity. The entropy production rate across the fixed vertical walls and the response of the walls to velocity and heat gradient evolution as well as the Bejan number field varies with an increase in the parameter values λ in a reactive exothermic chemical Powell-Eyring fluid. More also, the effect of activation energy term on the Bejan and entropy production is illustrated in the Figs. 17 and 18. A steady rise in the Bejan number is seen and a noteworthy increase is observed in the entropy generation. Activation energy is the energy needed for a reaction to occur, increasing the term ϵ spontaneously boosted the Bejan number and heat irreversibility distributions in the reactive non-Newtonian fluid.

Figs. 19 and 20 shows the impact of the Frank-Kamenenetskii term λ and electric field loading ϕ on the current density. Both terms rapidly enhances the current density in the channel walls by increasing the electric field conductivity effect of a hydromagnetic fluid flow. The parameters decreases the effect of Lorentz force as a result of magnetic field, hence the current density profiles rises. However, when $\phi = 0$ depicts the fluid distribution with short configuration circuit without electric field.

6. Conclusion

Investigation into the unsteady and inherent irreversibility of heat dependent electrical and thermal conductivities in a reactive Powell-Eyring fluid is carried out. It was noticed that, the fluid momentum and temperature increase or decrease correspondingly with a rise in the values of the parameters that increase or decrease the source terms. Also, it was computationally demonstrated, observed and reported that terms that strengthen the rate of entropy generation will congruently enhance the Bejan number. Hence, at low dissipation, viscosity and material variables the system irreversible process minimized the entropy generation. Therefore, to control or reduce the entropy generation during the process, the thermodynamic equilibrium needs to be improved and the viscous dissipative, inelasticity of the material, electric resistance, and magnetic hysteresis effects be discouraged. Moreover, it is seen that parameter λ that gives estimates on the critical regimes needs careful monitoring to avoid blowup of the reactive Powell-Eyring solution.

References

[1] N.S. Akbar, E. Abdelhalim, Z.H. Khan, Numerical analysis of magnetic field on eyring-powell fluid flow towards a stretching sheet, J. Magn. Magn. Mater 382 (2015) 355–358.

[2] M. Awais, T. Hayat, A. Alsaedi, S. Asghar, Time-dependent three-dimensional boundary layer flow of a Maxwell fluid, Comput. Fluids. 91 (2014) 21–27.
[3] S. Baag, S.R. Mishra, G.C. Dash, M.R. Acharya, Entropy generation analysis for viscoelastic MHD flow over a stretching sheet embedded in a porous medium, Ain Shams Eng. J. 8 (2017) 623–632.
[4] M.M. Bhatti, M.M. Rashidi, Numerical simulation of entropy generation on MHD nanofluid towards a stagnation point flow over a stretching surface, Int. J. Appli. Comput. Math. 3 (2017) 2275–2289.
[5] T. Chinyoka, O.D. Makinde, Viscoelastic modeling of the diffusion of polymeric pollutants injected into a pipe flow, Acta Mech. Sin. 29 (2) (2013) 166–178.
[6] R. Cortell, A note on flow and heat transfer of a viscoelastic fluid over a stretching sheet, Int. J. Non-Linear Mech. 41 (2006) 78–85.
[7] A.S. Eegunjobi, O.D. Makinde, Second law analysis for MHD permeable channel flow with variable electrical conductivity and asymmetric Navier slips, Open Phys. 13 (2015) 100–110.
[8] S.S. Ghadikolaeia, M. Yassaria, H. Sadeghia, Kh. Hosseinzadehb*, D.D. Ganjib, Analytical and numerical solution of non-Newtonian second-grade fluid flow on a stretching sheet Author links open overlay panel, Therm. Sci. Eng. Prog. 5 (2018) 309–316.
[9] S.S. Ghadikolaeia, Kh. Hosseinzadehb*, D.D. Ganjib, MHD raviative boundary layer analysis of micropolar dusty fluid with Graphene oxide (Go)-engine oil nanoparticles in a porous medium over a stretching sheet with joule heating effect, Powder Technol. 338 (2018) 425–437.
[10] M. Gholinia, Kh. Hosseinzadeha, H. Mehrzadib, D.D. Ganjia, A.A. Ranjbara, Investigation of MHD Eyring-Powell?uid?ow over a rotating disk under effect of homogeneous–heterogeneous reactions, Case Stud. Therm. Eng. 13 (2019) 100356.
[11] B.J. Gireesha, B. Mahanthesh, Perturbation solution for radiating viscoelastic fluid flow and heat transfer with convective boundary condition in nonuniform channel with Hall current and chemical reaction, ISRN thermodyn. 14 (2013) 481–490.
[12] A.R. Hassan, R. Maritz, The analysis of a reactive hydromagnetic internal heat generating poiseuille fluid flow through a channel, SpringerPlus 5 (2016) 1332.
[13] A.R. Hassan, R. Maritz, J.A. Gbadeyan, A reactive hydromagnetic heat generating fluid flow with thermal radiation within porous channel with symmetrical convective cooling, Int. J. Therm. Sci. 122 (2017) 248–256.
[14] A.R. Hassan, J.A. Gbadeyan, Entropy generation analysis of a reactive hydromagnetic fluid flow through a channel, U.P.B. Sci. Bull., Ser. A 77 (2) (2015) 285–296.
[15] T. Hayat, M. Awais, S. Asghar, Radiative effects in a three dimensional flow of MHD Eyring-Powell fluid, J. Egypt Math. Soc. 21 (2013) 379–384.
[16] T. Hayat, T. Muhammad, S.A. Shehzad, A. Alsaedi, Similarity solution to three dimensional boundary layer flow of second grade nanofluid past a stretching surface with thermal radiation and heat source/sink, AIP Adv. 5 (2015).
[17] T. Hayat, S. Nawaz, A. Alsaedi, Entropy generation in peristalsis with different shapes of nanomaterial, J. Mol. Liq. 248 (2017) 447–458.
[18] I.E. Ireka, T. Chinyoka, Non-isothermal flow of a JohnsonSegalman liquid in a lubricated pipe with wall slip, J. Non-Newton. Fluid Mech. 192 (2013) 20–28.
[19] M. Jalil, S. Asghar, S.M. Imran, Self similar solutions for the flow and heat transfer of Powell-Eyring fluid over a moving surface in a parallel free stream, Int. J. Heat Mass Transfer 65 (2013) 73–79.
[20] B.M. Jewel Rana, Raju Roy, Lasker Ershad Ali, S.F. Ahmmed, Radiation absorption and variable electrical conductivity effect on high speed MHD free convective flow past an exponential accelerated inclined plate, World J. Mech. 7 (2017) 211–241.
[21] R.A. Kareem, S.O. Salawu, J.A. Gbadeyan, Numerical analysis of non-Uniform heat source/sink in a radiative micropolar variable electric conductivity fluid with dissipation Joule heating, Am. J. Appl. Math. 6 (2) (2018) 34–41.
[23] M.A. Khan, M.I. Khan, T. Hayat, A. Alsaedi, Entropy generation minimization (EGM) of nanofluid flow by a thin moving needle with nonlinear thermal radiation, Phys. B: Condens. Matter 534 (2018) 113–119.
[24] P.M. Krishna, N. Sandeep, J.V. Ramana Reddy, V. Sugunamma, Dual solutions for unsteady flow of Powell-Eyring fluid past an inclined stretching sheet, J. Naval Architect. Mar. Eng. 13 (16) (2016) 89–99.
[25] B. Mahanthesh, J. Gireesha, R.S. Reddy Gorla, Eyring-Powell fluid past a convectively heated stretching sheet in the presence of thermal radiation, viscous dissipation and Joule heating, J. Assoc. Arab Univ. Basic Appl. Sci. 23 (2017) 75–82.
[26] R. Mahmood, S. Nadeem, N.S. Akbar, Oblique stagnation flow of Jeffery fluid over a stretching convective surface optimal solution, Int. J. Numer. Meth. Heat fluid flow 25 (2015) 454–471.
[27] O.D. Makinde, O.A. Beg, On inherent irreversibility in a reactive hydromagnetic channel flow, J. Therm. Sci. 19 (1) (2010) 72–79.
[29] O.D. Makinde, O. Franks, On MHD unsteady reactive Couette flow with heat transfer and variable properties, Cent. Eur. J. Eng. 4 (1) (2014) 54–63.
[31] M.Y. Malik, A. Hussain, S. Nadeem, Boundary layer flow of an Eyring-Powell model fluid due to a stretching cylinder with variable viscosity, Sci. Iran. 20 (2) (2013) 313–321.
[32] T. Mustafa, Anomalous heat transfer enhancement by slip due to nanofluids in circular concentric pipes, Int. J. Heat Mass Transfer 85 (2015) 609–614.
[33] T. Mustafa, Buongiorno model in a nanofluid filled asymmetric channel fulfilling zero net particle flux at the walls Author links open overlay panel, Int. J. Heat Mass Transfer 126 (2018) 974–979.
[34] M.M. Rashidi, S.A. Mohimanianpour, S. Abbasbandy, Analytic approximate solutions for heat transfer of a micropolar fluid through a porous medium with radiation, Commun. Nonlinear Sci. Numer. Simul. 16 (2011) 1874–1889.
[35] S.O. Salawu, Analysis of third-grade heat absorption hydromagnetic exothermic chemical reactive flow in a Darcy-forchheimer porous medium with convective cooling, WSEAS Trans. Math. 17 (2018) 280–289.
[36] S.O. Salawu, O. Adebimpe, A.M. Olanrewanju, Analysis of radiative heat absorption viscoelastic exothermic chemical reactive fluid with temperature dependent viscosity under bimolecular kinetic, Transylvan. Rev. 26 (32) (2018) 8339–8346.
[37] S.O. Salawu, A.M. Okedoye, Thermodynamic second law analysis of hydromagnetic gravity-driven two-step exothermic chemical reactive flow with heat absorption along a channel, Iran. J. Energy Environ. 9 (2) (2018) 114–120.
[38] M. Sheikholeslami, M. Jafaryar, Zhixiong Li, Second law analysis for nanofluid turbulent flow inside a circular duct in presence of twisted tape turbulators, J. Mol. Liq. 263 (2018) 489–500.

Further reading

[22] M.I. Khana, T. Hayata, M.A. Khan, A. Alsaedi, Activation energy impact in nonlinear radiative stagnation point flow of Cross nanofluid, Int. Commun. Heat Mass Transfer 91 (2018), 261–224.

[28] O.D. Makinde, T. Chinyoka, Numerical study of unsteady hydromagnetic generalized couette flow of a reactive third-grade fluid with asymmetric convective cooling, Comput. Math. Appl. 61 (2011) 1167–1179.

[30] O.D. Makinde, O.O. Onyejekwe, A numerical study of MHD generalized Couette flow and heat transfer with variable viscosity and electrical conductivity, J. Magn. Magn. Mater. 323 (22) (2011) 2757–2763.